Observation of atmospheric scintillation during the 2020 total eclipse in northern Patagonia

Christian T. Schmiegelow[1*], Martín Drechsler[1], Lautaro E. Filgueira[1],
Nicolás A. Nuñez Barreto[1] and Franco Meconi[2]

During the December 2020 total eclipse we registered time resolved light measurements of incident solar light with VIS-NIR photodiodes in northern Patagonia. Signals compatible with the observation of shadow bands in the 200 s before and after totality were observed. A strong increase in the normalized noise spectral densities of recorded incident radiation near totality suggests the presence of shadow bands. Originally high-altitude balloon measurements and spatial correlation ground measurements were planned, but the harsh climate conditions limited the campaign's results.

I Introduction

Total solar eclipses have long fascinated, intrigued and haunted humanity. These events, being so rare, are difficult to record and study. Moreover, uncontrollable meteorological conditions have a long-standing tendency of spoiling planned ground-based observations.

A quite common, but sometimes elusive, phenomenon called *shadow bands* occurs near the totality of solar eclipses. Minutes before and after totality, bands of randomly moving shadows may appear projected over the earth's surface. Over the past century many efforts were made to model [1–5] and to measure [6–11] these bands, and there are still open questions.

The most accepted explanation for shadow bands bases its analysis on different versions of atmospheric scintillation theories. For example, an early model based on inversion layers in the lower atmosphere was used by Gaviola to predict band size as

a function of the height of these layers [1]. More recent studies include a formal description of turbulence. Commonly, the models used are based on analysing propagation of light from an extended thin source (the sun almost covered by the moon) through air layers with different indices of refraction, with changing velocities and directions [2–4].

Shadow bands have typically been observed in the minute or two before and after totality, with characteristic wavelengths of a few centimeters, moving chaotically at average velocities in the low m/s range. Two principal observation methods have been implemented: video/photography and time resolved photovoltaic measurements of the light intensity at one or various correlated positions.

If shadow bands are indeed an atmospheric phenomenon, then they should not be observed at high altitudes above the troposphere. These altitudes are easily reached by low cost high-altitude balloons. Indeed, in several eclipses measurements were carried out from such balloons and from equivalent ground stations. The correlation between these measurements can help prove or debunk different proposed mechanisms and underlying models.

* schmiegelow@df.uba.ar

[1] Departamento de Física e Instituto de Física de Buenos Aires, FCEyN-UBA y CONICET, Argentina.
[2] "Terraza al Cosmos", Balboa 334, CABA, Argentina.

During the 2017 total eclipse observed in North America, such a correlated measurement was carried out by a team from the University of Pittsburgh [5]. There, a clear 4.5 Hz signal was observed during approximately 2 minutes before and after totality on all detectors, both ground and airborne (at a height of ≈ 25 km). The omnipresence of this signal may suggest that the origin of shadow bands is not exclusively due to atmospheric scintillations.

We designed a campaign to try and answer some of these questions during the 2020 total eclipse in northern Patagonia, spanning Argentina and Chile. Unfortunately, the campaign was strongly threatened by the weather conditions. Sparse clouds and high speed wind gusts over 60 km/h ruined some of the ground-based detectors and crashed the high-altitude balloon. However, with three working ground-based detectors, we were able to measure the characteristic chaotic spectrum. We did not detect any coherent signal at 4.5 Hz. Also, we were able to determine that the relative amplitude of the chaotic signal grows notoriously (at least ten times) in the minutes before and after totality, showing it is indeed an effect of the eclipse.

II Campaign and objectives

A campaign was designed to observe and analyse shadow bands during the 2020 eclipse in Patagonia. Time-resolved light intensity measurements, with both ground-based as well as airborne detectors, were planned. Due to climate inclemency, only some of the objectives were met. In this section, we describe the planned campaign, its objectives and the difficulties encountered.

On the 14th of December 2020, a total solar eclipse was to be seen across northern Patagonia at noon. We chose the City of Valcheta as base of observation site. This location was favorable as it was situated in the totality region, with a totality time of over two minutes, and the city administration was very enthusiastic and supportive to receive and host scientists during this event. Two missions were planned. One aimed at comparing the differences between ground- and high-altitude measurements, and another to test coherence at distances above 10 cm.

For the mission involving the high-altitude balloon, two identical detectors were built (see next section for details). One of the detectors was placed in the balloon payload, while the other was placed 1 m over ground, near the city of Valcheta (40° 41' 12.7" S, 66° 9' 43.3" W). The balloon was set to fly from the vicinity of the city of Sierra Colorada (40° 33' 59.1", S 67° 51' 29.3" W) which is roughly 140 km west of Valcheta. This election was made such that, at totality, the balloon would be flying roughly over Valcheta. The launch location was also chosen so that, when considering the winds during ascent and descent, the payload would land on firm land and not at sea, which is a demanding requirement in windy Patagonia.

The harsh weather conditions with gusts of over 60 km/h made one balloon burst before flight, and a spare one broke while ascending. This impeded the high-altitude measurements. Fortunately, the detector was recovered before the eclipse and was used as a ground station in Sierra Colorada (detector PDB). While windy, the sky over Sierra Colorada was clear, so this detector recorded the whole eclipse from 20 minutes before and up to 20 minutes after with no appreciable problems. Meanwhile, in Valcheta, where the original ground station (detector PDA) was placed, the sky was partially clouded, only clearing up somewhat during a short minute or two before totality, and 10 minutes later. Data from these two detectors was recovered successfully and is presented in the following sections, see Fig. 1.

At the Sierra Colorada location the total eclipse lasted 1 min 50.4 s; it occurred at an azimuth of 9.2° and was observed at an umbral depth of 47.88% (21.6 km), the path of totality having a width of 90.1 km. The Moon-Sun size ratio was 1.025 and the umbral velocity was 0.67 km/s. Correspondingly, at the Valcheta location, the umbral depth was 96.59% (43.4 km), with totality occurring at an azimuth of 1.6° and lasting 2 min 9 s. This data, which was used to plan the mission, was collected from the very complete web page on eclipses by X.M. Jubier [12].

A second, ground-based experiment was aimed at studying the spatial coherence of shadow bands beyond a few centimeters. A single acquisition system with two synchronized detectors was built for this purpose. The detectors (PDC and PDD) were placed 3 meters apart and 1 meter above the ground near the city of Valcheta. These detectors were also shadowed by the clouds before and after totality. The windy conditions partially disconnected

the ground cable of one of the detectors (PDD) rendering its data useless. The data from the remaining detector (PDC) was recovered but is not presented in the following sections, since its behavior is similar to PDA.

All data recorded is publicly available[1].

III Hardware

Detection units consisted of a non-polarized photodiode with a trans-impedance amplifier, an analog-to-digital converter (ADC) and a data storage system. Time tagging and storage was handled by an Arduino Mega microcontroller board. All systems were powered by two 4.2 V Lithium batteries in series, with an autonomy of more than 24 hours. All peripherals were embedded into the Arduino board via a shield, specifically designed for this purpose, and were supplied from the regulated 5 V source of the main board.

Two identical units with only one photodiode were produced. One was meant to fly on the balloon (PDB), the other to stay on ground (PDA). For these units we used a pair of Hamamatsu S 1226-BK, which were provided kindly by our colleagues at the University of Pittsburgh, to match what they used for the 2017 observation [5]. These photodiodes were directly soldered to the shield board.

A third unit, with two photodiodes, was also produced to measure time correlated signals at separate detectors. For these units we used two fast photodiodes, model VPW24r. The detectors were placed 2 m apart from each other and connected to the board by a 1 m long bipolar telephone cable.

The trans-impedance amplifier was designed to work optimally with a positive power supply and for the light levels expected at $\approx \pm 15$ min from totality. For this purpose a LM354 operational amplifier was chosen. To avoid problems at low light levels, a 90 mV bias voltage was applied in the non-inverting terminal of the amplifier such that the output of the amplifier is never near the ground rail [13]. The negative feedback network was composed of a 50 kΩ resistor in parallel with a 100 pF capacitor, giving a cutoff frequency of 31 kHz. The gain was chosen so that the amplifier would roughly

desaturate at the light level expected ≈ 15 minutes before totality.

As an ADC we used an ADS1115 chip, which has 16 bit resolution and was set to work at a sampling frequency of 250 Hz. Timing of measurements was handled independently by the ADC chip, which has an internal oscillator that handles timing when running in continuous mode. Time stamping of the measured readings was performed by the micro-controller with microsecond resolution following the system clock. As an extra absolute time reference, the readings of a real time clock with second resolution were recorded. Initially a higher sampling frequency was chosen (the chip's maximum is 860 Hz). However, at high sampling rates, we found the micro-controller would occasionally miss reading some samples. This happened when it was busy performing other tasks such as saving data to memory. At 250 Hz we found almost no missed measurements and a low jitter in recorded times. The unit with two detectors (PDC and PDD), worked with two ADCs each at a sampling frequency of 125 Hz, to ensure stable reading of both.

In all cases, the programmable gain amplifier of the ADC was set to unity, which gives a range of ± 4.096 V and a resolution of 125 μV. Although this amplifier could have been dynamically adjusted to have better resolution at low light levels, we opted for a more robust approach, which proved to work well.

The code used for the acquisition on the Arduino Mega board as well as the schematics of the circuits have been publicly released[2]. Future measurements should consider the following modifications or upgrades to the system: optimizing code or changing the microprocessor to allow for higher sampling rates and matching of the sampling rate with the filter of the trans-impedance amplifier to avoid aliasing.

IV Results

i Time Series

We begin the analysis of the recorded data by identifying characteristic behavior in the time series of light intensity recorded. Fig. 1 shows the recovered

---

[1] http://users.df.uba.ar/schmiegelow/eclipse2020

[2] https://code.df.uba.ar/schmiegelow/photodiode-data-logger
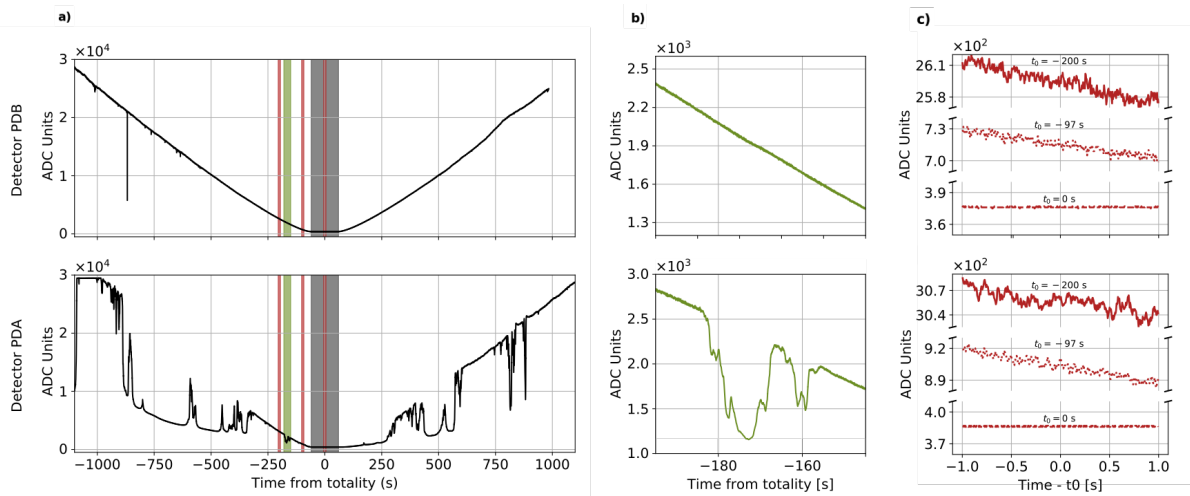
Figure 1: **Time series of the photodiodes signals.** (a) Whole time series of the balloon photodiode PDB (top), and a ground photodiode PDA (bottom). In grey shade, the totality of the eclipse. (b) Zoom of one of the moments when a cloud passed above the ground photodiodes, highlighted in green in the main plot. (c) Three zooms of three different moments of each signal, highlighted in red in the main plot.

values from the two relevant photodiodes PDA and PDB. In column a) we show a global view of the data recorded from $\approx$15 min before totality to $\approx$15 minutes after. The top plot (PDB) corresponds to the detector near Sierra Colorada, where there were no clouds. One sees the expected progressive light intensity reduction until totality, and then a smooth uncovering of the sun. Additionally, we see some short peaks, which we attribute mainly to dust and dirt flying by due to the hard winds. The second row shows the results from the detector near Valcheta (PDA). There, intermittent cloud coverage hindered most observation except for the few minutes before totality, where clouds partially cleared out. Cloud coverage can be seen as sudden drops of the light intensity measured. A detail of one of these events is shown in column b), which corresponds to the area shaded green in column a).

It is interesting to look at the fluctuations of the intensity, because these carry the information on the shadow bands. To do so, we start by observing the time resolved fluctuations in 1 second at different times from totality (T_n). Such details are shown in column c) of Fig. 1c for $t_0 = \{0, 97, 200\}$ s. All detectors show a clear reduction in absolute noise amplitude approaching totality. In both detectors PDA and PDB we observe that during totality the noise is at the level of the digitisation step (125 μV).

A detailed study of the time dependence of the noise densities is presented in the next section.

ii   Spectrograms and noise spectral density

We analyze the noise spectral density of the data acquired by the photodiodes at different time frames in a fashion similar to previous work [5,6].

To produce reliable and informative spectrograms, we proceed to normalize the signal in the following procedure: the time series of each photodiode is divided in chunks of 2048 points (this way, all chunks represent a time interval of $\approx$ 9 s). Then, each chunk is fitted by a linear function, which is used to normalize that group of data. By computing the discrete Fourier transform and taking the square of its absolute value, the noise spectral density of each chunk is obtained. In Fig. 2a-b we show the corresponding normalized and non-normalized spectrogram for the PDB data. The normalization plays two roles: 1) it removes the constant frequency component at ≈ 0.3 Hz, which is produced by the constant change in light intensity, and is not associated with shadow bands, and 2) it enhances / normalizes the relative noise to overall light intensity near totality. As seen in Fig. 2b the normalized data shows a strong increase of noise spectral density in the ≈ 200 s before and after totality, with a
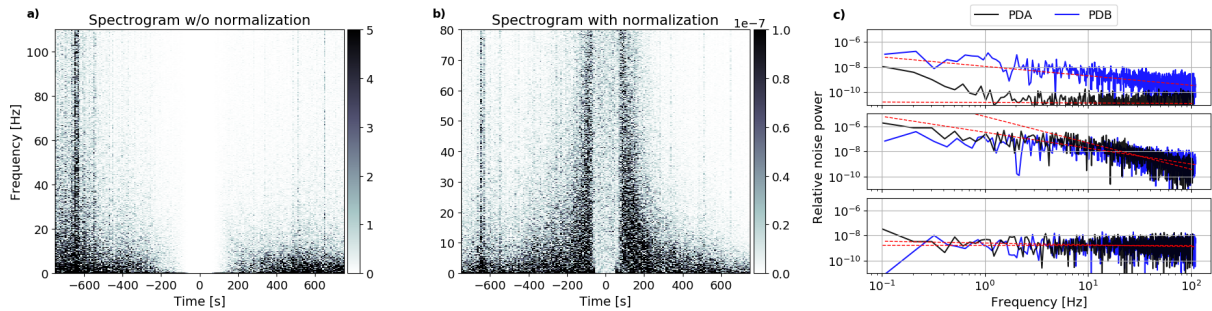
Figure 2: **Spectrograms and Power spectra at three different moments of the Eclipse.** a) Spectrogram of PDB signal, without any normalization. b) Spectrogram of PDB, with the signal normalized. c) Normalized power spectra in log-log scale calculated for N = 2048 points of PDA (blue) and PDB (black) at 550 s, 150 s and 0 s before totality. Linear fits to the are showed (red dashed), used to calculate the exponents for noise decay as in Fig. 3b. Noise power is calculated for each normalized chunk by computing the discrete Fourier transform and taking the square of its absolute value.

sharp drop when the sun is fully covered. This noise increase and sudden drop is the strongest evidence that the observed signal is a direct and unique consequence of the eclipse.

To quantify the change in noise figures, we fit spectra of each chunk with a power function. We find that all spectra are well represented by a simple power function from which we can extract the two characteristic numbers: the exponent and the power spectral density at a given frequency (we choose as a reference 1 Hz). A snippet of such fits is seen in Fig. 2c, where the noise spectral density is plotted in log-log scale for three characteristic moments of the normalized signal of both photodiodes. One before the shadow bands appear ($t = -550$ s), one when the phenomenon is occurring ($t = -150$ s) and the last one is during totality ($t = 0$ s). Comparing the first two cases, we see a clear increase of the noise intensity from around 10^{-8} to above 10^{-7} at 1 Hz. During totality, or during cloudy moments in PDA, the noise exponent drops to zero and the noise intensity drops a few orders of magnitude. This is consistent with the presence of shadow bands before and after totality, dominating the noise spectra during these time frames, while electronic noise appears to be the leading source of noise during totality.

We repeat this process for all chunks and plot both the exponents and relative powers as a function of time. This analysis is condensed in Fig. 3 for all data sets. As a reference, the first row a) shows the time-amplitude dependence. The noise expo-

nents, as a function of time are shown in Fig. 3b. We see a characteristic exponent between -1 and -1.5 for PDB, and between -1.5 and -1.8 for PDA, which is observed for all moments except when there is strong coverage by clouds or during totality, when the exponent tends to zero. We attribute the difference in exponents between detectors to a slight hardware difference, as we recorded compatible exponents for each detector on calibration runs with direct sunlight. Apart from this technical difference, detector PDB shows an interesting behavior approaching totality. The exponent seems to converge from a value in the vicinity of -1 away from totality to the lower -1.5 value near totality. Also, this behavior seems to be antisymmetric. We do not have a clear explanation for this. Background checks with both detectors under direct sun-light and on cloudy days showed fairly reproducible exponents with values compatible with each photodiode. Finally, we note that the exact value of this exponent was dependent on the frequency fit range and could vary between $-1.0(1)$ and $-1.3(1)$ for PDB between $-1.6(1)$ and $-1.8(1)$ for PDA and when varying the frequency range from 1 to 10 Hz in the lower limit of the fit. For all analysis here we used a frequency range of 1-100 Hz.

Finally, we discuss the behavior of the amplitude of the noise spectral density as a function of time. These results are shown in Fig. 3c. As a reference amplitude, we show the noise density at 1 Hz which is extracted from the fit to the individual normal-
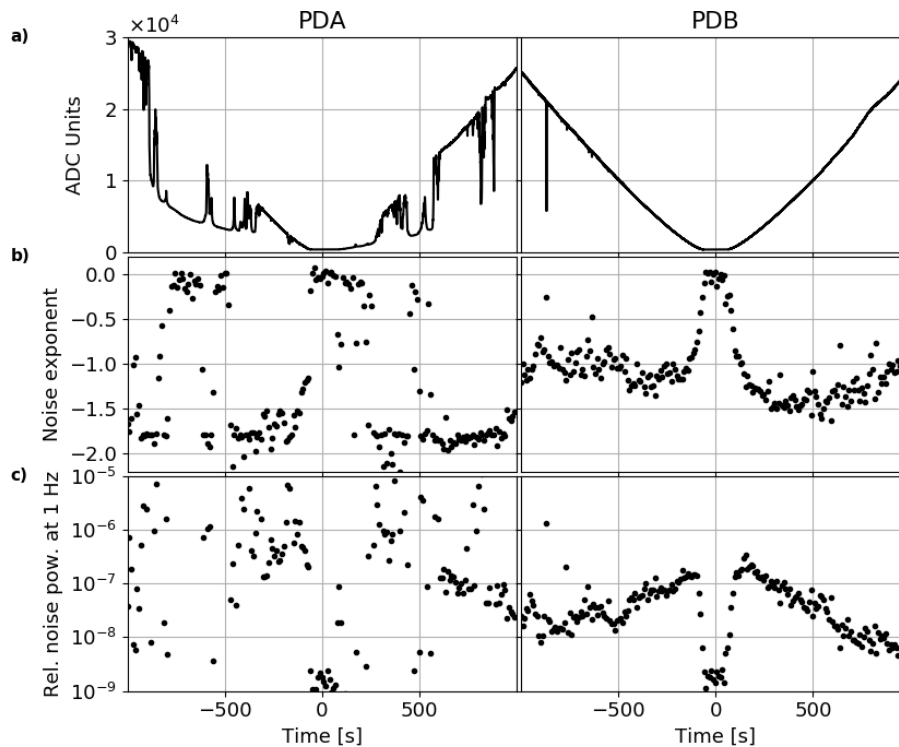
Figure 3: **Spectral properties of the measured time series.** a) The time series for each photodiode. Each signal is normalized in chunks of N=2048 points, and the noise exponent of the power spectrum for each of these chunks is plotted in b). The exponents are calculated by performing linear fits of each chunk in log-log scale. The value of this fit at 1 Hz is showed in c), giving the noise at that frequency as a function of time.

ized spectra. The clearest result is seen for detector PDB, where the absence of clouds allowed for a clean signal, and the increase in noise near totality can be seen. During totality, the noise amplitude drops to values compatible with zero. This increase and drop can also be guessed at in the moments before totality for detector PDA. However, in this case, the intermittent presence of clouds made the reading unreliable.

To confirm that the increase in noise spectral density is eclipse related, we tested our devices under similar lighting conditions. We placed the detectors under different sunlight conditions and controlled the light intensity over the detector using a combination of crossed plastic polarizers and neutral density filters. This allowed us to generate signals in all the range, from 1000 up to 30000 ADC units. In all cases, when lighting was on average stable (no strong clouds crossing by) we observed noise amplitudes below 10^{-8}, independent of signal

amplitude. This confirms that the increase of noise density in the 200 s before and after totality is indeed a signature of scintillation occurring because of the eclipse.

We close our analysis noting that none of the stations could reliably identify shadow bands with the eye or video cameras. It is not clear to us if they were difficult to observe because the weather conditions made observations difficult, or if these conditions indeed made the bands too fast, chaotic or small to catch them with the eye or camera.

V   Conclusions

By using time resolved measurements of light intensity on single photodiodes we were able to identify a clear signal compatible with the appearance of shadow bands with detectors at near sea level. The signal showed a strong increase in noise spectral density of the recorded signal in the ± 200 s

around totality with a strong drop during totality. The signals observed were all of chaotic nature, and no leading tone in the low frequency range was detected. The use of specially designed acquisition systems with sufficient time resolution, adequate calibration, memory and autonomy, allowed the recording of the onset and culmination of this effect with unprecedented completeness.

Future eclipses will provide new opportunities to repeat these measurements, accumulating evidence which will help us continue developing the understanding of this elusive phenomena, which only a few have been able to observe.

A final remark: as it is with field work, sometimes the great power of natural forces affects plans, which, if caught with time and wit, might be used to the experiment's favour. In this case, the best data was obtained by the detector that could not fly, and which, after balloon burst and payload recovery, was reconfigured and set to measure from ground.

[1] E. Gaviola, *On shadow bands at total eclipses of the sun*, Popular Astronomy **56**, 353 (1948).

[2] J. Quann and C. Daly, *The shadow band phenomenon*, Journal of Atmospheric and Terrestrial Physics **34**, 577 (1972).

[3] J. Codona, *The scintillation theory of eclipse shadow bands*, Astronomy and Astrophysics **164**, 415 (1986).

[4] H. Zhan and D. Voelz, *Wave optics modeling of solar eclipse shadow bands*, in 2019 IEEE Aerospace Conference, 1, IEEE (2019).

[5] J. P. Madhani, G. E. Chu, C. V. Gomez, S. Bartel, R. J. Clark, L. W. Coban, M. Hartman, E. M. Potosky, S. M. Rao, and D. A. Turnshek, *Observation of eclipse shadow bands using high altitude balloon and ground based photodiode arrays*, Journal of Atmospheric and Solar-Terrestrial Physics, **211**, 105420 (2020).

[6] L. A. Marschall, R. Mahon, and R. C. Henry, *Observations of shadow bands at the total solar eclipse of 16 February 1980*, Applied optics, **23**, 4390 (1984).

[7] B. Jones and C. Jones, *Shadow bands during the total solar eclipse of 11 July 1991* Journal of Atmospheric and Terrestrial Physics, **56**, 1535 (1994).

[8] D. Georgobiani, J. Kuhn, and J. Beckers, *Using eclipse observations to test scintillation models*, Solar Physics **156**, 1 (1995).

[9] B. W. Jones, *Shadow bands during the total solar eclipse of 3 November 1994*, Journal of Atmospheric and Terrestrial Physics, **58**, 1309 (1996).

[10] B. W. Jones, *Shadow bands during the total solar eclipse of 26 February 1998*, Journal of Atmospheric and Solar-Terrestrial Physics, **61**, 965 (1999).

[11] S. Gladysz, M. Redfern, and B. W. Jones, *Shadow bands observed during the total solar eclipse of 4 December 2002, by high-resolution imaging*, Journal of atmospheric and solar-terrestrial physics **67**, 899 (2005).

[12] X. M. Jubier, *Solar and lunar eclipses*, http://xjubier.free.fr/en/ Accessed: 2020-11-30.

[13] J. Caldwell, *1 MHz single-supply photodiode amplifier reference design*, TI designs precision: Verified design, **TIDU535-November**, 1 (2014).